Laser Interaction and Related Plasma Phenomena

Volume 10

Edited by

George H. Miley

Fusion Studies Laboratory
University of Illinois at Urbana–Champaign
Urbana, Illinois

and

Heinrich Hora

CERN
Geneva, Switzerland
and University of New South Wales
Kensington, New South Wales, Australia

PLENUM PRESS • NEW YORK AND LONDON

LASER PLASMA INTERACTION STUDIES RELEVANT FOR INERTIAL CONFINEMENT FUSION

O. Willi, T. Afshar-rad, M. Desselberger, M. Dunne, J. Edwards, L. Gizzi, F. Khattak, D. Riley, R. Taylor and S. Viana

Imperial College of Science, Technology and Medicine, London, UK

INTRODUCTION

Several basic processes occurring during the interaction of laser irradiation with matter have been investigated by using the high power laser systems of the SERC Central Laser Facility. The main effort of the recent research concentrated on ICF related studies with improved laser illumination uniformity generated by Random Phase Plate (RPP) Arrays and Induced Spatial Incoherence (ISI) techniques or a combination of both. In addition, highly transient plasmas have been produced by a prepulse-free 12 ps high power Raman shifted KrF laser pulse.

An interference code was written to predict the focal spot profiles produced by different smoothing techniques. Simulations were obtained at any time during the laser pulse and were compared to either time integrated or framed (framing time ≈ 140 ps) equivalent focal spot images. The predictions agree well with the experimental observations.

The suppression of instabilities including laser beam filamentation, stimulated Raman and Brillouin scattering was studied in large underdense plasmas with laser beams smoothed by RPP Arrays or ISI. Millimetre-sized cylindrical underdense high temperature plasmas were produced by irradiating thin foil targets with a number of laser beams in a line focus geometry. A separate laser beam interacted axially with the preformed plasma. Significant reductions in both the SRS and SBS levels were seen for both smoothing methods. In addition, time resolved x-ray and optical observations show whole beam self-focusing of the ISI beam in the preformed plasma.

The uniformity of the overdense plasma of laser irradiated targets was investigated by using a novel time resolved x-ray imaging technique with submicron spatial resolution. 2-D images show that laser beam nonuniformities imprint themselves onto the cold target surface at the beginning of the laser pulse generating considerable density perturbations which persist throughout and after the laser pulse with no evidence of smoothing.

Intense, soft x-ray pulses, generated from separate laser irradiated converters, were used to irradiate planar plastic foils. The x-ray heating was investigated by measuring the temperature histories of chlorinated tracer layers buried at different depths in the targets. The temperature diagnostic was a novel time resolved XUV absorption spectroscopy technique using chlorine L-shell transitions. The temporal temperature profiles were reasonably well reproduced by radiation hydrodynamic simulations.

Growth rates of the Rayleigh-Taylor instability were measured in thin foil targets with imposed sinusoidal modulations irradiated by optically smoothed laser beams. A hybrid optical smoothing scheme utilising ISI and RPP was used. The enhancement in the modulation depth during acceleration was observed with time resolved transmission radiography using a soft x-ray backlighting source. The wavenumber dependence and nonlinearity of the RT growth were investigated by using a range of modulation periodicities and depths. The measurements were compared with 2-D hydrocode simulations.

Finally, hot, close to solid density plasmas were produced by irradiating solid targets with a 12 ps 5 Joule Raman shifted KrF laser pulse. The power contrast ratio between the prepulse and the short pulse was less than 10^{-10}. X-ray and XUV observations show that the plasma is highly transient.

MODELLING OF FOCAL SPOT PROFILES BY AN INTERFERENCE CODE AND COMPARISON WITH EXPERIMENTAL RESULTS

In order to model the intensity profile produced by different smoothing techniques an interference code was written. The code solves the 2-dimensional, complex Kirchoff diffraction integral (KDI) in the Fresnel approximation and allows variation of the axial distance parameter to select different planes throughout the focal region. A Fast-Fourier-Transform algorithm is used to solve the integral. RPP and ISI behaviour is modelled using a Gaussian statistics routine to generate appropriate phase fronts. The code was used to predict focal spot intensity profiles at several times during the laser pulse for various smoothing techniques including RPP, ISI or a combination of both. The predicted profiles were compared with experimental equivalent plane images showing good agreement. Figure 1 shows the predicted focal spot profiles for ISI and ISI/RPP after 50 coherence times.

A full account of the results - including analysis of the degree of uniformity achieved and of the mode spectrum present in each case - is published elsewhere.[1] The possibility of employing rectangular-element RPPs for the production of high aspect ratio line-foci has also been investigated both experimentally and with interference code simulations. It is predicted that a square-topped profile can be achieved by adding a small bi-triangular phase-shift to the RPP-system. The method of combining such tilt elements with RPP elements of various shapes can be used to achieve almost any focal spot geometry. A rectangular-element RPP was used to generate a cylindrical plasma using a 12ps KrF laser pulse suitable for x-ray laser research.[2]

STUDY OF INSTABILITIES IN LONG SCALELENGTH PLASMAS WITH AND WITHOUT LASER BEAM SMOOTHING TECHNIQUES

The interaction of intense laser light with large underdense plasmas is of great interest for inertial confinement fusion since fusion pellets will be surrounded by large plasma coronas. Under these conditions various parametric instabilities such as Stimulated Brillouin Scattering (SBS), Stimulated Raman Scattering (SRS) and laser beam filamentation may be very effective, resulting in the reduction of laser plasma coupling, in the production of high energy electrons and in the nonuniform heating of the plasma corona. To simulate fusion conditions, plasmas with scalelengths of about one millimetre were recently produced by focusing four green laser beams of the Rutherford Appleton Laboratory high power glass laser system onto thin foil targets in a line focus configuration.[3] A delayed green laser beam was focused axially into the preformed underdense plasma with an electron temperature and density of about 0.5 keV and 0.1 n_c respectively (n_c is the critical density for

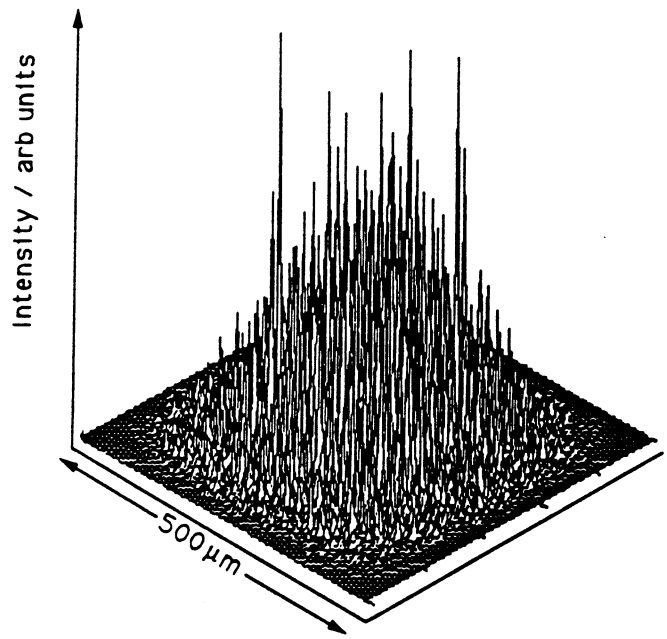

Figure 1a. Predicted intensity profile of an RPP laser beam after 50 coherence times.

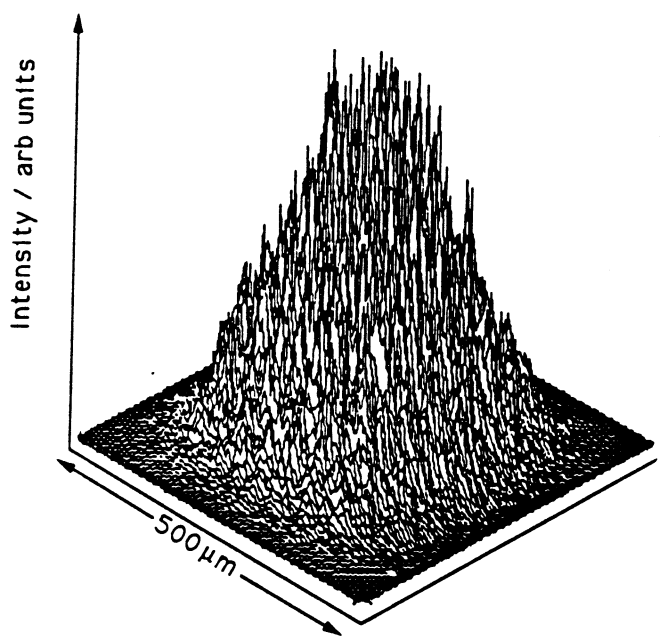

Figure 1b. Predicted intensity profile of a RPP/ISI smoothed laser beam after 50 coherence times.

the interaction beam).[4] Significant levels of SRS were seen and laser beam filamentation[5] and whole beam selfocusing[6] were clearly observed. On some of the interactions, when whole beam self-focusing was seen, anomalously large SBS shifts were observed which are difficult to explain in terms of classical SBS. A simple model of self phase modulation is invoked which in combination with SBS can explain the experimental observations.[7] When the incident laser beam was smoothed either by a RPP or ISI a significant reduction in the absolute levels of these instabilities and the virtual suppression of filamentation were seen.[8,9]

In this paper experimental results of a recent investigation are reported. The preformed plasma was again formed by a line focus configuration using four heating beams. However the heating beams were also smoothed by ISI in contrast to previous measurements in order to produce a more uniform preformed plasma. Either an ISI smoothed infrared (1.05 μm) laser beam or a broadband beam delayed by 2.2 ns was focused axially into the preformed plasma. An intensive set of diagnostics was used to investigate the plasma conditions of the preformed plasma and the nonlinear interaction of the laser beam with the plasma.

The model plasma was generated by irradiating a thin aluminium foil target (700 nm thick, 0.7 mm long, 300 μm wide) which was overcoated on a 100 nm thick formvar substrate. Two pairs of opposing green laser beams smoothed by ISI were superimposed in a line focus configuration as heating beams to form the plasma. Typical irradiances of 10^{14} Wcm^{-2} were used. A separate infrared laser beam typically delayed by 2.2 ns was used to interact with this plasma along its longitudinal axis. Measurements were made either with the broadband beam ($\sim\omega/\omega \simeq 0.1$ %) or with an ISI laser beam. At the time of interaction the nominal electron density of the preformed plasma was about 0.3 n_c and the electron temperature about 500 eV. The uniformity of the preformed plasma was investigated transversely to the exploding foil target by using optical Moire deflectometry techniques with a probe wavelength of 350 nm. The density profile was measured interferometrically with the 350 nm probe beam propagating along the axis of the preformed plasma. The electron temperature of the plasma was obtained from time resolved x-ray streak spectroscopy. The backscattered Brillouin signal generated by the interaction beam was imaged out via the incident focusing lens onto a calibrated photodiode. In addition, time resolved SBS spectra were recorded with an S1 optical streak camera. A four frame x-ray pinhole camera with a gating time of about 150 ps was used to observe the x-ray emission of the preformed plasma and of the interaction beam.

Figure 2 shows the absolute levels of SBS backscattering for the ISI and broadband interaction beams as a function of the incident irradiance.[10] The focal spot of the interaction beam was 140 μm in diameter and was kept constant for all the data shots. For the broadband laser beam a threshold at an irradiance of about 3×10^{13} Wcm^{-2} is observed with a saturation level between 2 to 6 % of the incident laser energy. For the ISI interaction beam an exponential behaviour is seen with an average SBS value of 0.5 % at an irradiance of 7×10^{14} Wcm^{-2}. The SBS backscattering levels are significantly higher than observed in a previous experiment[8,9] in which a green interaction beam was used, the plasma was less uniform and the electron density was lower (by about a factor of 3) during interaction. However, even if similar electron densities to those obtained previously are used (by irradiating a 500 nm target), the SBS levels observed remain at the same high levels seen with the 700 nm targets. The estimated electron density is consistent with backscattered SRS which was detected by diodes filtered with narrowband interference filters. For the 700 nm targets virtually no SRS backscatter is

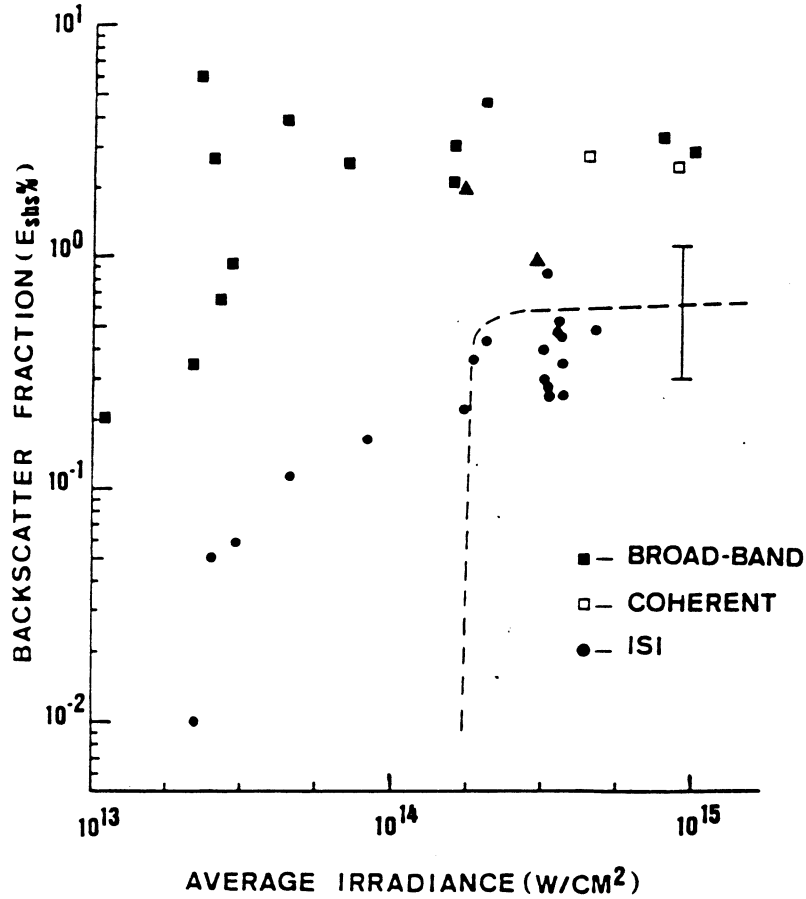

Figure 2. Variation of SBS backscatter fraction with average irradiance for an infrared ISI (illustrated by the solid circles) and broadband (squares) interaction beam. Also shown are the SBS levels for green coherent interactions.

observed. On the other hand, clear SRS signals (at a wavelength of about 1.5 μm) are seen with the 500 nm targets. For comparison, the dashed line in figure 2 represents the SBS levels for green coherent interactions. It is important to note that the SBS levels for the green ISI interactions were below the detection threshold.[8]

For some of the data shots the first experimental evidence of whole beam self-focusing of an ISI laser beam was obtained.[11] For these particular shots the target thickness and "heating" irradiance were adjusted to produce a more collisional interaction. This was achieved by exploding a thinner Al foil target (500nm thick, 0.35mm long, 300μm wide) with a reduced "heating" irradiance I_H=3.5x10^{13}Wcm^{-2}. The effect was to produce a preformed plasma with a similar peak electron density of 0.3n_c but with a reduced electron temperature of 300 eV at t_D=1.7ns. The result of the cooler plasma conditions will be to enhance the strength of the thermal self-focusing mechanism (γ_{TH}) which is strongly temperature dependent, $\gamma_{TH} \sim T_e^{-5}(N_e/N_c)^2$.

Fig.3 shows a sequence of three x-ray framing images (140ps gate-time) of the preformed plasma taken with the gating period of the framing camera

ending 1ns before the interaction, 50ps before the peak of the pulse and 150ps after the peak of the pulse respectively. The interaction irradiance was $I_{av}=2.5x10^{14}Wcm^{-2}$. As can be seen in figures 3b and 3c a strong filamentary channel has formed with a transverse scalelength of less than 50μm in diameter, ie. this is significantly smaller than the beam at the plasma input-plane. At the exit-plane we also observe a strong emission plume extended beyond the exit, which is consistent with hot plasma being expelled from a filament channel by the beam break-out. Further confirmation was provided by optical probing images taken simultaneously with the x-ray records where a density cavity at the input was seen. In addition, the SBS backscattered signal increased by a factor of 8 for these shots compared to the data taken with similar irradiances where no self-focusing was observed.

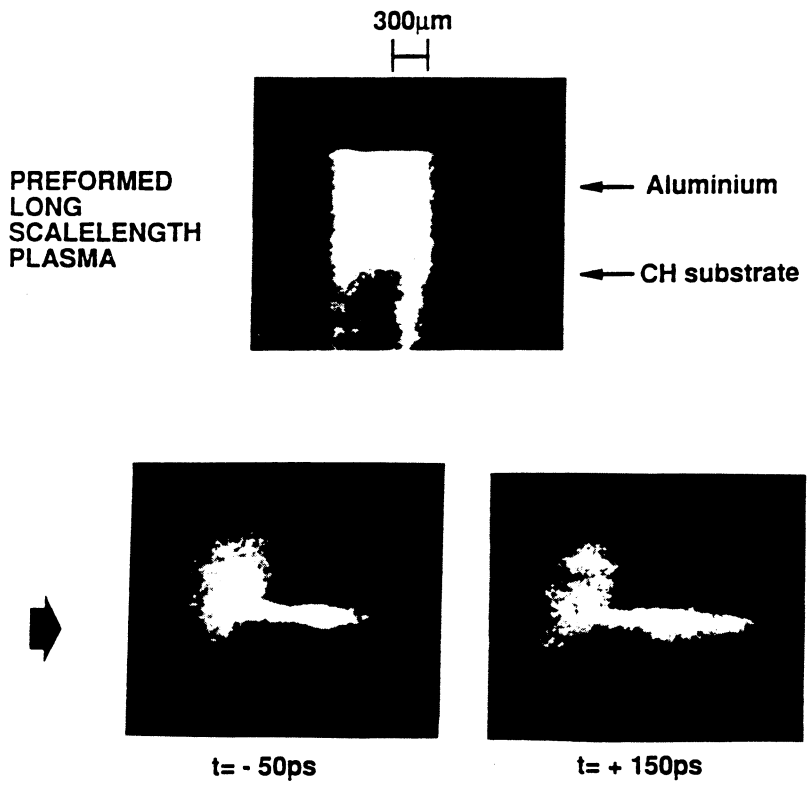

Figure 3. A time sequence of x-ray framing images (140ps gate-time) recording the preformed plasma a) 1ns before the start of the pulse b) 50ps before the peak of the pulse and c) 150ps after the peak of the pulse. The interaction beam delay $t_D=1.7ns$ with $N_e\simeq0.3N_c$ and $T_e\simeq300eV$. The average interaction irradiance $I_{av}=2.5x10^{14}Wcm^{-2}$, focal-spot size=140$\mu$m. A strong emission channel is clearly identified in Figs.3b and 3c consistent with beam self-focusing.

INVESTIGATIONS OF THE UNIFORMITY OF OVERDENSE PLASMAS BY XUV PROBING TECHNIQUES

After the first experimental evidence of jet formation in the underdense plasma corona of laser irradiated targets was provided using optical probing techniques,[12,13] considerable theoretical interest was stimulated. A number of mechanisms for the production of the jet-like structures have been proposed in theoretical studies. For a review see Ref. 14.

Until now, no experiment has however clearly identified the responsible mechanism, nor has any evidence been obtained of the effect of these instabilities on the ablation rate or on thermal smoothing. Of particular

importance to the ICF programme is the question of whether the jets exist only in the subcritical region (all experimental work until now has provided information only about the subcritical region) or whether they extend into the supercritical region, where their effects are potentially far more detrimental for implosion symmetry. It is of paramount importance to investigate the superdense region for the occurrence of these instabilities with good spatial and temporal resolution.

A novel experimental techniques based on only recently available multilayered mirror technology for use in the XUV spectral region has been developed.[15] As it is well known, optical probing is limited to the sampling of relatively low density regions $n_e < n_c$, since the optical rays are refracted out of the imaging optics by the steep plasma density gradients. Shorter wavelengths are refracted less and simulations show that XUV probe wavelengths approximately of 100 A will, in combination with the imaging effectively probe the conduction region up to several times critical density.

The imaging system consists of a spherical mulitilayered mirror operating at a wavelength of 130 A with a bandwidth of about 20 A. The overall magnification of the system was about 50x. The spatial resolution has been measured by using a zone plate as an object and was found to be about 0.8 μm, limited by the resolution of the microchannel plate intensifier which was used as a detector. The temporal resolution was 150 ps which was the gating time of the microchannel plate detector. A higher spatial resolution was achieved when Kodak 101-01 film was used. The mirror images the self-emission and also the shadow of the expanding plasma generated by either a short pulse (100ps) x-ray backlighter flash (produced by irradiating a separate gold target using another beam) when film was used as a detector or by a long pulse x-ray backlighter (1.5 ns) when the microchannel plate detector was used.

The uniformity of the overdense plasma was investigated by irradiating thin gold and Cu wire targets with coherent, ISI and ISI/RPP smoothed laser beams.[16] Figures 4a and b show two images taken on 101-01 film showing the effect of ISI and ISI+RPP hybrid irradiation (in these experiments, beam energy levels were adjusted to provide constant irradiation at $\simeq 5 \times 10^{13}$ Wcm^{-2} for direct comparison). For the target in Fig. 4a, a 20μm gold wire, defocussed ISI irradiation from an aspheric f/10 lens is incident from the left and provides regularly spaced spikes of intensity (corresponding to the individual beamlets). These generate jets of blow-off plasma which persist throughout and after the pulse (the backlighter frame is taken at 2.3ns after the peak of the drive pulse). In the same image, tight-focussed ISI irradiation from an identical lens is incident from the right. In this latter case, all the beamlets are overlapped and the time-integrated profile is smooth. From the image, however, it is evident that the blow-off is not uniform with jets of material similar to those observed in the defocussed case. The structures are no longer regular since, in the case of completely overlapped beamlets, the nonuniformity in the focal spot is of a random nature. From this image, it is evident that laser focal spot nonuniformities - present only over timescales short compared to the laser coherence time - imprint themselves onto the target at these early times. This imprint initiates density nonuniformities which are never smoothed out thereafter. Figure 4b shows an image also taken on 101-01 film, with hybrid RPP+ISI irradiation incident on a 10μm gold wire (again at an irradiance of 5×10^{13} Wcm^{-2}). The small-scale ($\simeq$10μm) speckle structure produced by the RPP is smoothed by the ISI action over many coherence times. In Figure 4b, structure on the scale of the speckle is clearly observed and persists throughout the pulse and thereafter as in the case of the ISI-only irradiation (Figure 4a). In this case the structure appears to be regular since it is on the scale of the RPP speckle. As with the ISI-only case one is lead to the conclusion that, at early times, the laser structure imprints itself onto the target, initiating nonuniform ablation.

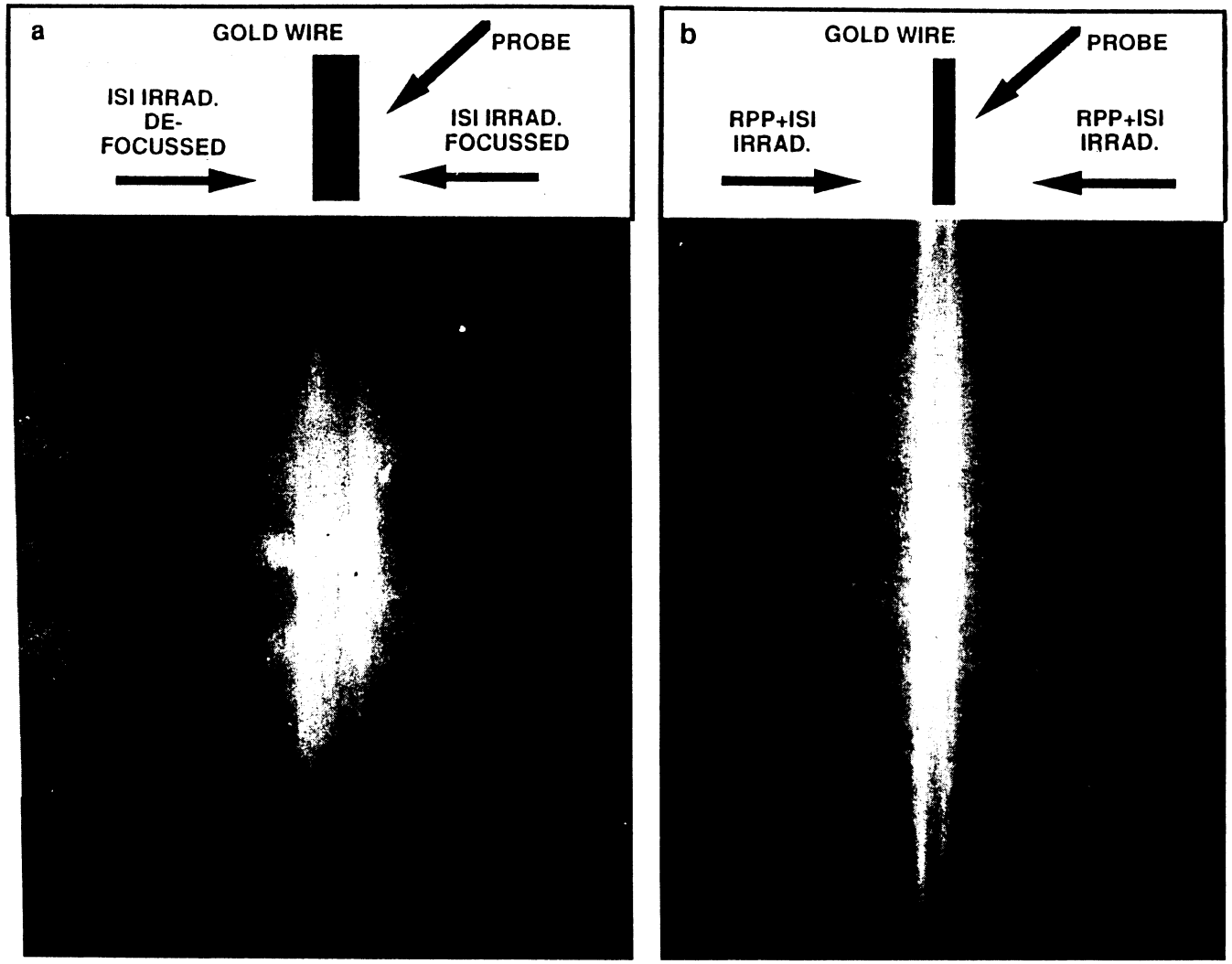

Figure 4. **(a)** A 20μm Gold wire is irradiated from the left by defocussed ($\simeq$ 250μm from best focus, into the beam near-field) and from the right by tight-focussed ISI radiation. In both cases f/10 focussing optics was used with λ=0.53μm and I$\simeq$5x10^{13}Wcm^{-2}. Regularly spaced nonuniformities (corresponding to the individual beamlets) are clearly observed on the defocussed ISI side (left). On the tight-focussed ISI side (right) nonuniformities are also still clearly visible, although these are now of a random nature since all the beamlets are overlapped.

(b) A 10μm Gold wire irradiated by RPP+ISI hybrid radiation from both sides (I$\simeq$5x10^{13}Wcm^{-2}, λ=0.53μm). Gross nonuniformities in the self-emission and blow-off plasma are clearly visibvle in the X-ray image. In both Figs. 4 a,b the backlighter frame is taken 2.3ns after the peak of the main pulse. The white arrows indicate the initial left- and right-hand edges of the target.

The effects of radiation imprint on the plasma formation was tested with uniform irradiation. A uniform plasma was observed with an intense source of soft x-rays which was produced by irradiating a separate foil target. This foil consisted of a 1000 Angstrom plastic (parylene, C_8H_8) substrate overcoated with 500 Angstroms of gold. Two green beams (incident at an angle of 30 degrees to the normal of the foil) are used to irradiate the foil at an intensity of about 10^{14} Wcm^{-2}. The x-rays produced by the gold plasma are transported through the thin plastic substrate. This is ablated away during the pulse and, apart from serving as a substrate for the gold deposition, also absorbs the remainder of the optical pulse after this burns through the gold. The foil was placed at a distance of 250μm from the wire target, providing an estimated irradiance (in x-rays) of 10^{13} Wcm^{-2} under our conditions. The question is whether such a uniform plasma can be used to thermally smooth intensity nonuniformities in an incident laser beam avoiding the initial imprint problem. This question was investigated by irradiating a Cu wire target with a soft x-ray drive. An ISI laser beam delayed by 1.2 ns was used to interact with the preformed plasma. It was evident from the observations that there were no visible jet-like structures, neither in the self-emission nor in the backlit plasma indicating that thermal smoothing of the nonuniformities in the interaction beam had occurred.

MEASUREMENT AND ANALYSIS OF RADIATION TRANSPORT IN RADIATIVELY HEATED FOIL TARGETS

The transport of soft x-ray radiation through thin foil plastic targets, up to 6μm thick, was recently studied using time resolved XUV spectroscopy in the 10 to 70 Å region. An intense source of x-ray radiation was produced by overcoating the front side of the target with 100nm of gold and irradiating it with green laser light at an intensity between 1 and $5x10^{14}Wcm^{-2}$. The soft x-rays transmitted through the target were diagnosed by a time resolved, grazing incidence flat field spectrometer coupled to an XUV streak camera.[17] The experiments were simulated with a multi-group radiation transport model which was coupled to a hydrodynamic code. Overall agreement was obtained between the experimental observations and the simulations. In detail, however, a smaller shift in the carbon K-edge was observed experimentally in transmission during heating than predicted theoretically.[18] These measurements were extended by using a separate burnthrough foil target to generate an intense source of soft x-rays. The soft x-rays transmitted through the burnthrough target were used to heat the thin plastic foils. Absorption spectra observed in the region of the carbon K-edge using a time resolved flat field spectrograph indicated that the smaller shift seen experimentally in the carbon K-edge is due to the presence of bound-bound transitions not included in the initial calculations.[19] In this paper we report on measurements of temperature profiles as a function of time and depth in plastic foil targets heated by an intense soft x-ray source using a novel time resolved XUV absorption spectrocopy technique.[20]

Thin plastic foil targets were heated by an intense Pseudo-Planckian source of soft x-ray radiation. The x-ray radiation was generated by illuminating a separate target consisting of a thin 100 nm gold layer which was supported on a 1μm plastic substrate with six frequency doubled RPP smoothed beams (800 ps in duration) of the VULCAN laser arranged in a cluster configuration. The focal spot was typically 500 μm (FWHM) in diameter as measured with an x-ray pinhole camera. The soft x-ray radiation transmitted through the burnthrough target was used to heat a separate planar CH foil, positioned parallel to the burnthrough foil and separated from it by approximately 250μm. A thin chlorinated tracer layer ($C_8H_6Cl_2$), 0.3μm thick, was buried at different depths in the CH foil targets. The soft x-rays transmitted through the target were analysed using a time resolved, grazing incidence flat field spectrometer coupled to an XUV streak camera. The

temporal and spectral resolutions were aproximately 50 ps and 0.3 Å respectively. The soft x-ray radiation was reflected into the spectrograph by a pair of highly polished silica mirrors acting as a high frequency cut off filter for x-rays with energies above approximately 600 eV to reduce multiple order effects.

Numerical simulations were carried out using a multi-group radiation transport model coupled to the 1-D Lagrangian hydrodynamics code MEDUSA. The radiation transport code uses 116 groups in the 0-100keV energy region. Group averaged Planck mean opacities are used and are calculated at the material temperature, in-line with the hydrodynamics using an average-atom (AA) screened-hydrogenic approximation in LTE, based on the model XSN. Only bound-free and free-free transitions are considered in the model. The behaviour of the laser irradiated thin gold layer was not calculated in the code because of the marked non-LTE behaviour of the x-ray emitting region of the gold plasma which could not be accurately calculated by our LTE model and so an experimentally measured heating spectrum was used instead. Small inaccuracies in the gold spectral emission do not cause any serious errors in the material heating, with simulations including the M, N and O band emission not predicting any significant differences in the overall results. The x-ray conversion efficiency from the burnthrough target was estimated from time-resolved and time-integrated XUV photodiode measurements taken under similar experimental conditions when a value of $5.5\mp2\%$ was found. The value used in the 1D simulations was adjusted to give best agreement with the experimental measurements to account for the geometrical coupling of the source emission to the target and variations in the conversion efficiency.

Detailed spectral analysis of the experimental data has been performed using a spectral analysis package (SAP) containing an extensive atomic data base (oscillator strengths, level and transitions energies) generated by a multi-configuration Dirac-Fock atomic physics code. In the calculation of the transition energies, the initial and final atomic states are optimised separately. Ionic distributions are calculated with the Saha equation. The lineshape is taken to be Lorentzian. Synthetic absorption spectra are generated from the calculated opacities by solving the time-dependent equation of transfer in one dimension for a given plasma density, temperature and thickness. The predicted spectrum is convolved with the instrumental function, in this case taken to be Gaussian with a FWHM given by the instrument resolution. Plasma conditions are inferred by comparing the predicted spectra with those observed experimentally. Calculations were performed for the tracer layer only. The remainder of the target introduces no discontinuous absorption features in the energy range of interest and only affects the slope of the underlying continuum as verified when targets with no tracer layers were used. The analysis is based mainly on 2p-3d transitions of F-like to S-like chlorine ions.

Targets with $0.3\mu m$ tracer layers buried $0.2\mu m$ and $1.8\mu m$ below the surface of a $2\mu m$ CH target were irradiated with an x-ray flux of between $2\text{-}5\times10^{12}Wcm^{-2}$. Several distinct differences between the two target configurations were observed. When the chlorinated layer is placed $0.2\mu m$ below the front surface of the target, the 2p-3d transitions shift towards shorter wavelength more rapidly than when the layer is positioned at a depth of $1.8\mu m$ (rear layer) indicating a more rapid ionization of the material in the front layer. This can also be seen from the earlier turn on of Na-like and Ne-like absorption features (by $\simeq$200-300ps) in the spectrum from the front layer. In addition, the chlorine becomes more highly ionized in the front layer indicating that a higher temperature is attained here. This can be seen from the appearance of F-like absorption features approximately 500ps after the start of the x-ray pulse. In contrast, little evidence is seen for the presence of significant fractions of F-like ions in the rear layer. Also, the 2p-3d

Na-like absorption feature remains prominent for the layer at the rear of the target whereas it becomes almost unnoticeable after about 900ps when the layer is positioned near the front surface.

The temperature histories of the tracer layers were inferred as a function of time by comparing the experimental data with detailed, synthetic, absorption spectra calculated by SAP. Calculations were performed for the temperatures between 5 and 50eV at 5eV intervals and for densities between 1 and 0.005g/cc with the ratio between successive values of aproximately 2. Figure 5 shows a comparison between a densitometer trace taken approximately 900ps after the start of the emission from the front layer spectrum and an absorption spectrum caclulated with SAP for a density of 0.02g/cc and a temperature of 40eV. For comparison, a trace taken across the spectrum produced by the chlorinated layer positioned near the rear of a plastic target is also shown. Figure 6 shows a comparison between the temperature histories inferred from the absorption spectra and those predicted by the radiation hydrocode using the "best fit" x-ray conversion efficiency of 2.5%. The solid curves show the range of temperatures predicted by the hydrocode to exist in the tracer layers. The vertical error bars on the experimental points include the estimated uncertainty in the inferred temperature both due to the discrete density and temperature values at which the synthetic spectra were calculated and due to spatial gradients in the layers parallel and perpendicular to the target surface. For reference, the x-ray pulse shape is also shown in figure 6.

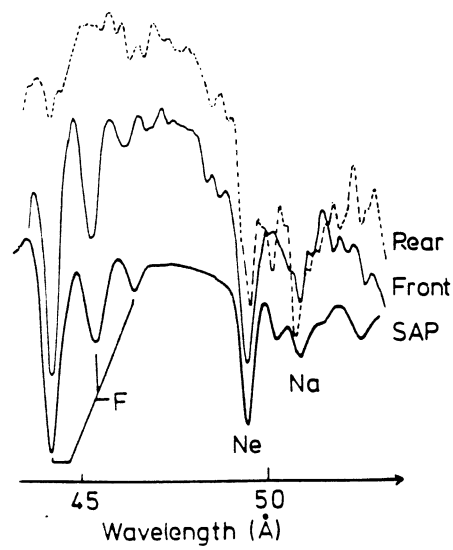

Figure 5. Traces taken near the peak of the emission and a spectrum predicted by SAP for 40eV and 0.02g/cm^3. Some 2p-3d transitions are marked. For clarity the spectra have been displaced vertically.

The overall agreement between the experimentally measured points and the hydrocode simulations is reasonably good. In particular, the different shapes of the temporal profiles for the front and rear layers are reproduced well. In the simulations, the rear layer is "preheated" (0-400ps) to temperatures above that of the ambient CH by radiation mainly in the carbon window below the K-edge where the intervening CH is optically thin. A significant fraction of the x-rays in this region is absorbed in the chlorinated

layer due to b-f chlorine L-shell transitions. As the layer heats and ionizes, its opacity in the carbon window region decreases as the chlorine L-shell b-f threshold shifts towards higher energy. As a result the layer heating rate is reduced and a temperature plateau is established (400-800ps). The intervening CH is heated mainly by x-rays in the energy regions just above and well below the carbon K-edge where the photon mean free path is sub-micron. As the material is ionized, the opacity is reduced and, in particular in this case, the K-edge shifts towards higher energy allowing radiation in this region to propagate into the cooler material where it is strongly absorbed. It is the propagation of this "ionization front" that is responsible for the step in the simulated rear layer profile at around 850ps. Similar behaviour is not predicted for the front layer because the 0.2μm of the intervening CH is optically thin to the source over most of the photon energy spectrum and therefore, will have little effect on the layer heating.

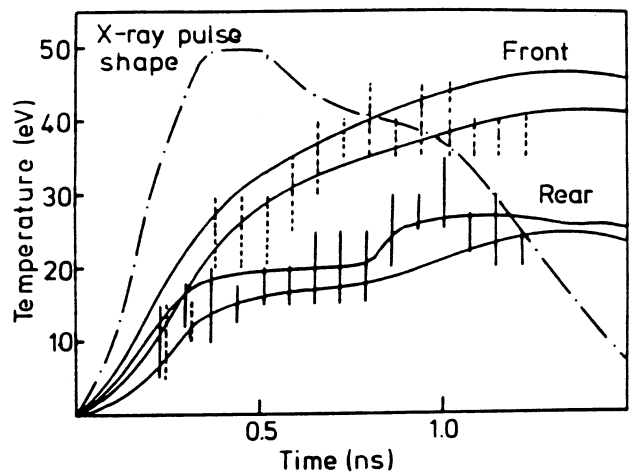

Figure 6. Comparison of experimentally measured temperature histories and those predicted by the radiation hydrocode. The x-ray pulse shape is shown.

STUDY OF RAYLEIGH TAYLOR INSTABILITY USING X-RAY BACKLIGHTING TECHNIQUES

The Rayleigh-Taylor instability occurs in any accelerating fluid system in which the density and pressure gradients are of opposite sign. In the case of ICF experiments, the hot, low density ablating plasma accelerates a cooler, more dense part of the target and is thus succeptible to the RT instability. In an ICF implosion small imperfections in the target manufacture or intensity nonuniformities present in the laser irradiation may initiate RT growth sufficient to disrupt the target symmetry to an unacceptable degree. Here we describe experimental measurements in which the growth rates of the Rayleigh-Taylor instability were measured in thin foil targets with imposed sinusoidal modulations irradiated by optically smoothed laser beams. A hybrid optical smoothing scheme utilising ISI and RPP was used. The enhancement in the modulation depth during acceleration was observed with time resolved transmission radiography using a soft x-ray backlighting source. The wavenumber dependence and nonlinearity of the RT growth were investigated by using a range of modulation periodicities and depths. The measurements were compared with 2-D hydrocode simulations.[1,21]

Six frequency doubled green (0.53μm) beams arranged in a hexagonal cluster with a cone angle of 13 degrees, were focused onto thin foil targets with f/10 lenses. The six superimposed beams generated a smooth, flat-topped spatial intensity profile providing uniform acceleration across the target surface. The total energy delivered on target was approximately 250 Joules with a pulse duration of 1.76 ns (FWHM) resulting in an incident irradiance of about 1.5×10^{14} Wcm^{-2}. This was kept constant throughout the experiment to allow direct comparison of the results for different target specifications. The laser beams were smoothed by a hybrid scheme consisting of Induced Spatial Incoherence (ISI) and Random Phase Plate (RPP) arrays. The ISI was generated using a broad-band oscillator ($\Delta\omega/\omega$=0.1%) and a 6x6 echelon to produce 36 independent beamlets. The RPP's were placed immediately in front of each of the six focusing lenses. In addition to profile smoothing, the RPP's have the effect of increasing the far-field focal spot size to a large (approx. 335 μm) diameter. An x-ray pinhole camera, filtered for an x-ray energy band between 0.84 keV and 1.63 keV was used to monitor the uniformity of the focal spot produced by the drive beams. Intensity variations of about 1% (calculated with a 2D weighted averaging procedure) were seen over a spatial wavelength of 10μm. The far field focal spot distribution was calculated using an interference code. This showed close agreement to the experimentally determined profile structure and uniformity.

The targets consisted of low density ($0.9g/cm^3$) (CH_2) plastic approximately 16μm thick with sinusoidal modulations of periodicity 30μm, 50μm, 70μm and 100μm. Modulation depths between 1.8μm and 4.6μm were investigated, with the modulations always facing the drive beams. The accelerated targets were backlit with a Mg backlighter source which was generated by a separate green laser beam 2.5 ns in duration. The transmitted fraction of the x-rays produced by the backlighter source was imaged onto a streak camera by means of a pinhole with an overall spatial resolution of 21 μm. The image was filtered for a spectral wavelength window between 0.84 and 1.63 keV containing the magnesium Heα and Lyα transitions. The backlighter spectrum was measured using a time-integrated crystal spectrometer with filtering identical to that used in front of the streak camera. From this the relative contribution to the image intensity at each wavelength in the backlighter could be determined. Control experiments with only the drive irradiation (to determine the contribution to the image caused by self-emission from the target) and with backlighter illumination only were conducted. In addition to the transmission radiographs, streaked edge-on radiographs were recorded to obtain the target acceleration.

Computer simulations of the experiment were performed using the 2D Eulerian hydrodynamics code POLLUX which has been extensively tested under various conditions. The code was modified to incorporate the sinusoidal target surface modulations and matched to the experimental conditions by varying the absorbed irradiance until the inertial motion measured in the experiment was reproduced in the simulations. The absorbed intensity was chosen as the variable parameter, since it is the least well-characterised experimental quantity due to the effects of lateral energy transport. It was found that approximately 50% of the energy needs to be absorbed to reproduce the experimentally determined inertial motion. This value is comparable to previous measurements under similar conditions.

From the transmission radiographs the ripple amplitude growth rates were determined by microdensitometry of the streak records to give quantitative measures of the observed X-ray contrast levels at different times. Both the initial modulation depth and the instability growth rate were then deduced from exponential curves fitted to the data. The growth rates measured in this way are plotted in figure 7 as fractions of their classically predicted values, the errors representing the spread of the amplitude of modulation evident at late times. The measured initial (t=0) modulation depth were convolved with the modulation transfer function (MTF) of the imaging system and compared

to the known initial modulation depths (accurately measured by microscopy before the experiment). No significant discrepancy was found (error < 0.4μm). Further, no growth rate analysis was carried out during the initial period in which the shock passes through the target. In this time, the growth is not due to the RT instability but due to the shock driven Richtmeyer–Meshkov instability.

Also plotted in figure 7 are the measured growth rates of the NRL experiment[22] and those predicted by the POLLUX simulations (for both high and low modulation depths) and the predictions for high modulation depth targets after convolution with the MTF of the imaging system. Several points arise. Firstly, the qualitative wavelength dependence of the observed growth rates is in fair agreement with the dependence predicted by the simulations; growth was observed at all modulation periodicities including 50μm. Secondly, the growth rates predicted by the simulations are (except for two points) outside the error bars and greater than the observed rates. This may not be purely due to the

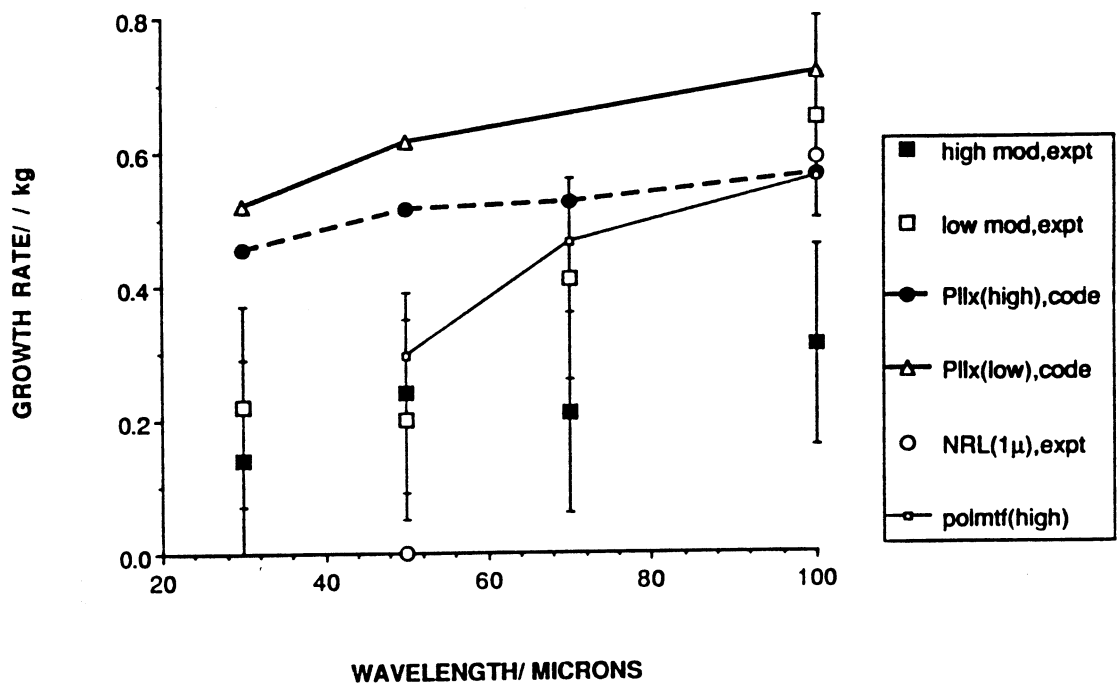

Figure 7. Measured RT growth rates presented as a fraction of the classical growth rate $(kg)^{1/2}$ where k is the modulation wavenumber and g is the acceleration for both high (4.5 μm) and low (2.6 μm for 30 μm and 50 μm periodicity; 1.8 μm for 70 μm and 100 μm periodicity) modulation depth targets. Also shown are POLLUX results for 1.8 μm (low) and 4.5 μm (high) modulation depth targets, MTF-corrected POLLUX results for high modulation depth targets, and experimental results from [Ref. 22].

nonlinearity of the growth, but may in part be due to radiation transport effects not included in the modelling. These would, in principle, reduce the growth rate. The excitation of higher order modes also reduces the growth rate of the fundamental. To investigate the extent of such higher-order contributions to the growth of the instability, the X-ray radiographs were spectrally analysed with a Fourier decomposition package. It was found that small amplitude higher order modes are clearly present at late times (≈1.6ns after the start of the laser drive pulse) for 100μm modulation periodicity targets. Such higher harmonic modes were not clearly observed in the case of

the 50μm targets, where only the fundamental mode was found to have a significant Fourier component (for the case of 30μm targets, the resolution of the imaging system was insufficient to detect higher harmonic growth).

PLASMA PRODUCTION WITH 12 ps HIGH POWER UV LASER PULSES

The interaction of short pulse and wavelength lasers with solid targets is of great interest for various areas in plasma and atomic physics. Since the laser energy is absorbed close to the initial target surface a large thermal conduction wave is launched into the solid material before hydrodynamic expansion occurs resulting in the formation of a hot, close to solid density plasma.[23] Besides fundamental studies of plasma and atomic physics, these plasmas are of great interest as pump media for X-ray lasers.[24] In addition, plasma conditions may be generated in the laboratory which are interesting for astrophysical applications. We have recently carried out studies of plasmas produced by irradiating various solid targets with a 3.5 ps KrF laser pulse.[24-27] Here we report on observations of plasmas produced by irradiating targets with a 12ps KrF laser pulse at an intensity up to $1x10^{17}$ Wcm^{-2}. The contrast ratio between the prepulse and the short pulse intensity was less than 10^{-10} resulting in an irradiance of the prepulse which is well below the threshold for forming a pre-plasma.

The experiment was carried out at the SERC Central Laser Facility using the short pulse, high power KrF system SPRITE.[28,29] A KrF pulse was amplified in a series of KrF amplifiers and Raman shifted in methane resulting in a wavelength of 268 nm. A total laser energy of about 5J in a pulse 12ps in duration was obtained. The laser beam was focused onto planar targets with an f/4 parabolic mirror. With a focal spot of 10 μm (FWHM) in diameter, irradiances of about $1x10^{17}$ Wcm^{-2} were obtained on the target surface. Time resolved X-ray spectroscopy was used to diagnose the plasma. A curved TLAP crystal in a Johann configuration was coupled to an x-ray streak camera covering a spectral range between 5 to 7 A. The temporal resolution was about 15 ps.

Figure 8 shows an x-ray streak record taken on an aluminium target which was irradiated at an intensity of about $1x10^{16}$ Wcm^{-2}. As can be seen in the spectrum the aluminium transitions are very broad, particularly during the laser pulse. Also, the higher series members such as Heϵ are not observed. This spectral behaviour is characteristic for emission originated from very high density plasmas. The electron density of the emitting region of the plasma was calculated as a function of time by comparing the experimental line widths of Heγ and Heβ from the time resolved data with those predicted by the atomic physics code RATION and SPECTRA. The main broadening mechanism is Stark although it was estimated that about 15% of the line width is caused by opacity broadening. A peak electron density of about $1.5x10^{23}$ cm^{-3} was obtained for a bare aluminium target. Electron densities up $3x10^{23}$ cm^{-3} were obtained for targets with an aluminium layer buried below a plastic layer 0.2μm in thickness and irradiated at an intensity of about $5x10^{16}$ Wcm^{-2}. The electron temperature is obtained from the Heβ:Lyβ line ratio of spectra recorded under similar experimental conditions. Because of the short time scales involved, the plasma is highly transient, especially at early times. To check the validity of using a steady state atomic physics code the 1-D hydrocode simulations were post processed with a time-dependent, average atom model. Both the time dependent and steady state ionisation stage populations were calculated. It was seen that the time dependent analysis gives a distinctly different temperature profile compared to the steady state interpretation. Electron temperatures up to 800 eV are obtained with the time dependent analysis whereas a maximum temperature of about 600 eV is estimated with the time independent analysis. The time dependent interpretation seems to be more consistent with the experimental observations

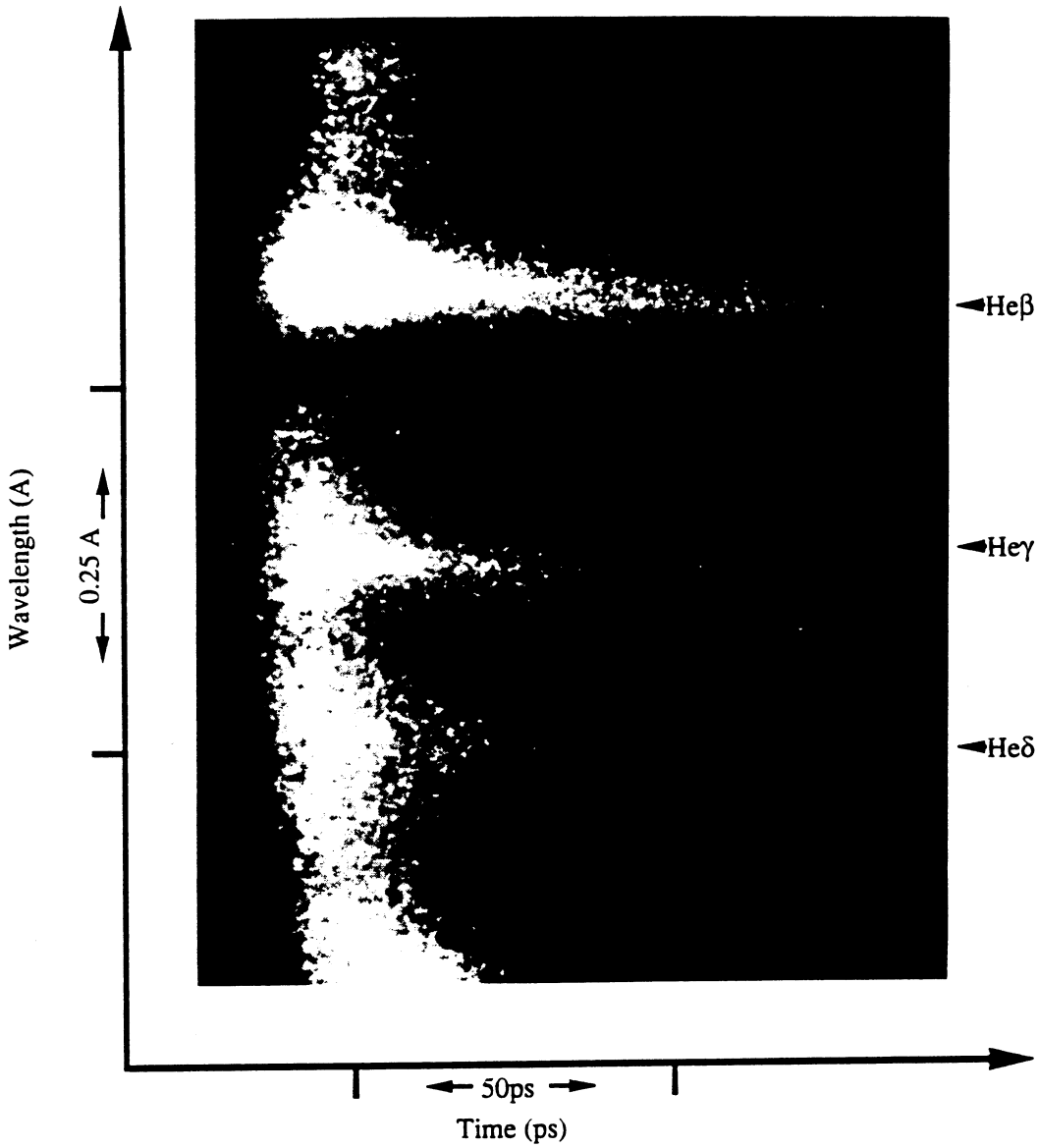

Figure 8. Time resolved spectrum obtained when an aluminium target was irradiated at an intensity of about $1x10^{16}Wcm^{-2}$.

since hydrogenic like chlorine emission was seen on KCl targets irradiated at similar intensities.

The experimental conditions were modelled with the 1-D Lagrangian hydrocode MEDUSA. The ions are assumed to have a perfect gas equation of state (EOS), while the electrons are described by a Thomas Fermi EOS with modifications to give the correct solid density. The ionisation balance of the plasma is calculated with a time dependent average atom approximation in NLTE. The laser energy was absorbed via inverse bremsstrahlung and 5% of the remaining laser energy was dumped at the critical density surface to simulate resonance absorption. A flux limiter of 0.1 was used in the simulations since this value agreed best with measurements taken on plastic coated aluminium targets. Simulations of these targets under the same conditions, but with a flux limiter of 0.03, revealed that the temperature would not be hot enough to ionise the target to hydrogenic like aluminium wheras a flux limiter of 0.1 would. For these conditions MEDUSA predicts an absorption of 30%.

CONCLUSIONS

In summary this paper gives a review of our ICF related work carried out during the last two year. The main effort of the research concentrated on studies with improved laser beam uniformity. The interaction of a smoothed laser beam with large underdense homogeneous plasmas and solid targets was investigated. It was seen that the levels of SRS, SBS and filamentation were suppressed when smoothed laser beams were used. It was also observed, however, that the large initial nonuniformity present in smoothed laser beams imprint themselves onto the cold target surface early in the laser pulse. A novel hybrid scheme was proposed where a uniform plasma is formed with an intense soft x-ray source. The preformed plasma is then irradiated with a smoothed laser beam avoiding the initial imprint. The heating of foil targets by soft x-rays was investigated experimentally and computationally. The Rayleigh-Taylor growth was studied in targets driven by combination of ISI and RPP smoothed laser beams. Finally, highly transient plasmas were generated with a prepulse-free 12 ps, 0.268 μm laser pulse.

ACKNOWLEDGEMENTS

The authors thank the staff of the Central Laser Facility for their assistance and technical support. This work was funded by several SERC grants. We would like to acknowledge the contributions made by Dr. A. Giulietti to the long scalelength interaction experiments and by Dr. S. Rose to the radiation transport studies.

REFERENCES

1. M. Desselberger and O. Willi, submitted to Phys. Fluids B.

2. M. Desselberger, L Gizzi, V. Barrow, J. Edwards, F. Khattak, S. Viana, O. Willi and C. Danson, Appl. Optics, March 1992.

3. S. Coe, T. Afshar-rad, D. Bassett, J. Edwards and O. Willi, Opt. Commun. 81, 47 (1991).

4. O. Willi, D. Bassett, A. Giulietti and S. Karttunen, Opt. Commun. 70, 487 (1989).

5. S. Coe, T. Afshar-rad and O. Willi, Opt. Commun. 73, 299 (1989).

6. S. Coe, T. Afshar-rad and O. Willi, Europhys. Lett. 13, 251 (1990).

7. T. Afshar-rad, S. coe; A. Giulietti, D. Giulietti and O. Willi, Europhys. Lett. 15, 745 (1991).

8. S. Coe, T. Afshar-rad, M. Desselberger, F. Khattak, O. Willi, A. Giulietti, Z. Q. Lin, W. Yu and C. Danson, Europhys. Lett. 10, 31 (1989).

9. O. Willi, T. Afshar-rad, S. Coe and A. Giulietti, Phys. Fluids B 2, 1318 (1990).

10. T. Afshar-rad, M. Desselberger, L. Gizzi, O. Willi, F. Khattak and A. Giulietti, submitted to Phys. Rev. Lett.

11. T. Afshar-rad, L. Gizzi, M. Desselberger, F. Khattak, O. Willi and A. Giulietti, accepted in Phys. Rev. Lett.

12. O. Willi, P. Rumsby and S. Sartang, IEEE J. of Quant. Electr. QE-17, 1909 (1981).

13. O. Willi, P. Rumsby, C. Hooker, A. Raven and Z. Lin, Opt. Commun. 41, 110 (1982).

14. M. G. Haines, Can. J. Phys. 64, 914 (1986).

15. M. Desselberger, T. Afshar-rad, F. Khattak, S. Viana and O. Willi, Appl. Optics 30, 2285 (1991).

16. M. Desselberger, T. Afshar-rad, F. Khattak, S. Viana and O. Willi, submitted to Phys. Rev. Lett.

17. G. Kiehn, T. Garvey, R. Smith, O. Willi, A. Damerell and J. West, Proc. SPIE Int. Soc. Opt. Eng. 831, 150 (1987).

18. J. Edwards, V. Barrow, O. Willi and S. Rose, Europhys. Lett. 11, 631 (1990).

19. J. Edwards, M. Dunne, L. Gizzi, O. Willi, S. Rose, C.A. Back and C. Chenais-Popvics, Proceedings of the Sarasota Workshop on the Properties of Hot Dense Matter (World Scientific, Singapore, to be published).

20. J. Edwards, M. Dunne, D. Riley, R. Taylor and O. Willi, Phys. Rev. Lett. 67, 3780 (1991).

21. M. Desselberger, O. Willi, M. Savage and M. Lamb, Phys. Rev. Lett. 65, 2997 (1990).

22. J. Grun et al., Phys. Rev. Lett. 58, 2672 (1987).

23. O. Willi, T. Afshar-rad, V. Barrow, J. Edwards and R. Smith, Proc. of the International Conference on LASERS' 89, edited by D.G. Harris and T. M. Shaw, STS Press, McLean, VA, 40 (1990).

24. R. A. Smith, V. Barrow, J. Edwards, G. Kiehn and O. Willi, Appl. Phys. B 50, 187 (1990).

25. O. Willi, G. Kiehn, J. Edwards, V. Barrow and R. Smith, OSA Proc. on Short Wavelength Coherent Radiation: Generation and Applications, edited By R. Falcone and J. Kirz, Vol. 2, 194 (1988).

26. O. Willi, G. Kiehn, J. Edwards, V. Barrow, R. Smith, J. Wark and E. Turcu, Europhys. Lett. 10, 141 (1989).

27. J. Edwards, V. Barrow, O. Willi and S. Rose, Appl. Phys. Lett. 57, 2086 (1990).

28. M. Steyer, I. Ross and J. Lister, Annual Report to the Laser Facility Commitee 1990, RAL-90-026, 90 (1990).

29. E.C. Harvey, C.J. Hooker, J.M. Lister, I.N. Ross, M.J. Shaw, G.J. Hirst, M.H. Key, P.A. Rodgers and J.E. Andrew, Annual Report to the Laser Facility Committee 1990, RAL-90-026, 79 (1990).